







Article

Au/ZnO Nanocomposites Prepared by Laser Ablation for Enhancement of Antibacterial Activity and Cytotoxic Properties against Cancer Cells

Muhanad Alhujaily ^{1,*}, Majid S. Jabir ^{2,*}, Uday M. Nayef ², Taha M. Rashid ², Ghassan M. Sulaiman ^{2,*}, Khalil A. A. Khalil ^{1,3}, Muntadher I. Rahmah ⁴, Mazin A. A. Najm ⁵, Rihab Jabbar ² and Sabrean F. Jawad ⁶

¹ Department of Medical Laboratory Sciences, College of Applied Medical Sciences, University of Bisha, Bisha 67714, Saudi Arabia

² Department of Applied Sciences, University of Technology, Baghdad 10066, Iraq

³ Department of Medical Laboratory Sciences, Faculty of Medicine and Health Sciences, University of Hodeidah, Hodeidah 3114, Yemen

⁴ Department of Medical Physics, College of Science, Al-Karkh University for Science, Baghdad 10011, Iraq

⁵ Department of Pharmaceutical Chemistry, College of Pharmacy, Al-Ayen University, Nasiriyah 64001, Iraq

⁶ Department of Pharmacy, Al-Mustaqbal University College, Hillah 51001, Iraq

* Correspondence: malhujaily@ub.edu.sa (M.A.); 100131@uotechnology.edu.iq (M.S.J.); ghassan.m.sulaiman@uotechnology.edu.iq (G.M.S.)

Abstract: This study presents a comprehensive look into the potential therapeutic, antibacterial, and anticancer properties of a nanocomposite (NC) of gold (Au) and zinc oxide (ZnO). In this study, we analyzed the adherence between Au nanoparticles (NPs) and ZnO NPs. X-ray diffraction analysis showed high crystallinity and small crystallite sizes of Au NPs and ZnO NPs, while transmission electron microscopy showed spherical NPs. Furthermore, histogram analysis showed that the average particle size of Au NPs is 27 nm, while that of ZnO NPs is 35 nm. The adherence of ZnO NPs on the surface of Au NPs increased their combined particle size to 51 nm and revealed a high-population core-shell structure. The activity of Au/ZnO NCs against *Escherichia coli* was more potent when compared to that of elemental Au and ZnO NPs alone. The cytotoxic effects of Au NPs, ZnO NPs, and Au/ZnO NCs against human breast cancer cells (AMG13) and human esophageal adenocarcinoma cancer cells (SK-GT4) were investigated in this study. We found that AMG13 is more sensitive than SK-GT4 to the activity of Au/ZnO NCs. The cytotoxicity of Au/ZnO NCs against AMG13 was 89%, while that against SK-GT4 was 85%. Less cytotoxic effects were recorded against normal cells (MCF7) when compared with those of cancer cells. Based on these findings, the synthesized Au/ZnO NCs could be used as a promising strategy for biomedical applications.

Keywords: laser ablation; Au NPs; ZnO NPs; *E. coli*; cytotoxic activity



Citation: Alhujaily, M.; Jabir, M.S.; Nayef, U.M.; Rashid, T.M.; Sulaiman, G.M.; Khalil, K.A.A.; Rahmah, M.I.; Najm, M.A.A.; Jabbar, R.; Jawad, S.F. Au/ZnO Nanocomposites Prepared by Laser Ablation for Enhancement of Antibacterial Activity and Cytotoxic Properties against Cancer Cells. *Metals* **2023**, *13*, 735. <https://doi.org/10.3390/met13040735>

Academic Editors: Antonio Riveiro Rodríguez and Pavel Krakhmalev

Received: 23 January 2023

Revised: 26 March 2023

Accepted: 4 April 2023

Published: 9 April 2023



Copyright: © 2023 by the authors. Licensee MDPI, Basel, Switzerland. This article is an open access article distributed under the terms and conditions of the Creative Commons Attribution (CC BY) license (<https://creativecommons.org/licenses/by/4.0/>).

1. Introduction

Nanotechnology is the study of manipulating substances on the atomic and molecular scale, as well as the synthesis and application of materials with dimensions in the order of a billionth of a meter (10^{-9} m = 1 nm) [1,2]. Proteins, enzymes, nucleic acids, viruses, secondary metabolites, antibodies, and other biological molecules are all parts of molecular materials. By self-assembly in benign and environmentally safe conditions, these can also be used to create complex materials. The goal is to produce novel materials by fusing natural compounds with manmade or nonbiological components for applications outside of biology [3]. The biomedical, pharmaceutical, agricultural, and industrial sectors have all made substantial use of biodegradable nanomaterials. Several techniques have been developed for synthesizing nanomaterials, including sol-gel [4], sputtering [5], and laser ablation (LA) [6,7]. The LA technique has been widely used to prepare noble metal nanoparticles (NMNPs). The synthesis of gold (Au) nanoparticles (NPs) via LA is a simple

method for creating new phases of nanomaterials that can involve both liquid and solid phases. Additionally, this method does not require extreme temperature and pressure conditions, making it an eco-friendly, chemically straightforward, and clean method [8], favorable in the preparation of NMNPs, particularly Au NPs. The NPs' average size and distribution can be adjusted by adjusting the laser fluence, wavelength, and salt concentration [9].

Hyperthermia, gene therapy, magnetic targeting, environmental remediation, pigments, catalysts, antimicrobial agents, and soil treatment are just some of the many uses for gold/zinc oxide (Au/ZnO) nanocomposites (NCs). In order to achieve high purity without resorting to difficult purification techniques that might necessitate the removal of harmful chemicals used in the manufacturing process, Au/ZnO NCs were prepared via the LA technique [10]. Rashid et al. created Au:ZnO core-shell NPs. Their results showed that the particle size increased with the energy levels and that the surface shell of ZnO on Au NPs had a significant impact on absorption [11,12]. In a process involving LA, Au and ZnO NPs were prepared. The results demonstrated that the antibacterial agent Cur-Au:ZnO in the prepared sample caused the bacterial cells to die by breaking down their cell walls and entering the cytoplasm. As a photoelectrode material, Au:ZnO presented a higher photocurrent density than pure ZnO NPs under simulated sunlight, as described by Shao et al. [13]. A wide variety of internal and external factors could contribute to the DNA damage brought on by nanomaterials in bacteria. One way that ROS can be created is through the use of internal assaults. ROS are created during regular cellular metabolism. These free radicals are extremely unstable, so when they come into contact with other molecules, the reactions occur very quickly. When free radicals come into contact with DNA, they set off a chain reaction that leads to the formation of genotoxic lesions. Examples of what are known as external agents include pharmaceuticals, as well as gamma, ultraviolet, and X-ray radiation. NPs have the potential to cause exogenous DNA damage. Previous studies have been conducted on the effects of nanomaterials on bacteria, but more research is required to better understand the effectiveness of nanoparticles on pathogenic bacteria [14]. The dispersion of most chemotherapeutic agents throughout the body, which can result in general toxicity and limited tolerance by patients, presents various challenges for traditional chemotherapy as a method of cancer treatment. Due to their ability to silence genes and deliver drugs, metallic nanoparticles (NPs) such as Ag-ZnO constitute a potentially useful platform for the treatment of cancer. In addition, they have the ability to be functionalized by targeting ligands, which can reduce the growth of tumors and eventually cause them to become damaged. Due to the high purity of the produced nanoparticles in an aqueous solution, the technique of laser ablation has become an appealing method for fabricating and forming nanomaterial and nanoparticles. This is because the technique results in the formation of only pure nanomaterial and nanoparticles in the solution, with no other substances being formed [15]. It has been demonstrated that ZnO NPs have an extraordinary capacity to generate oxidative stress in cancer cells. When it comes to increasing the susceptibility of cancer cells' ZnO NPs' cytotoxicity, this is one of the processes that plays a role. This property can be attributed to ZnO's status as a semiconducting material. ZnO is what causes the production of reactive oxygen species (ROS), which in turn causes oxidative stress, which ultimately can lead to cell death if the cells' own antioxidative capacities are overwhelmed. Herein, we prepared Au NPs, ZnO NPs, and Au/ZnO NCs via LA. Characterizations of their shape and size were undertaken by transmission electron microscopy (TEM), ultraviolet-visible (UV-Vis) spectrophotometry X-ray diffraction (XRD), and Fourier transform infrared spectroscopy (FTIR). We studied the antibacterial activity of Au NPs, ZnO NPs, and Au/ZnO NCs against *Escherichia coli*, and their cytotoxicity against human breast cancer cells (AMG13) and esophageal cancer cells (SK-GT4) using an MTT assay. Our findings suggested the ability of Au NPs, coated with ZnO NPs and prepared by laser ablation, to enhance antibacterial and anti-proliferative roles against cancer cells.

2. Materials and Methods

2.1. Materials and Reagents

High-purity gold (Au) was modified to create a bright-yellow disk with a diameter of 15 mm and a thickness of 2 mm (Sigma, St. Louis, MO, USA). Zinc (Zn), at a purity of 98%, was ordered as a powder from VWR International, Radnor, PA, USA, then pressed by hydraulic pressing at a pressure of 10 T for 10 min to obtain a pellet with a diameter of 16 mm and a thickness of 3 mm. Roswell Park Memorial Institute (RPMI-1640), methyl thiazolyl tetrazolium (MTT), trypsin-EDTA, fetal bovine serum (FBS), crystal violet stain, acridine orange, and ethidium bromide were obtained from Sigma, St. Louis, MO, USA. Penicillin and streptomycin were purchased from Biosource International, Nivelles, Belgium. However, the other reagents and chemicals used in the current study were employed in their analytical grades.

2.2. Preparation of a Colloidal Solution of Au/ZnO NCs

An Au plate was immersed in 3 mL of deionized water (DW) in a glass vial and ablated with 1064 nm pulses from an Nd:YAG laser running at 1 Hz with a pulse length of 9 ns. The ablation was performed for 200 pulses with a laser energy of 800 mJ directed at the target, with a few modifications to the ablation process, as described in [16]. The LA technique was performed without any movement of the target. Then, 3 mL of DW was added to a glass beaker with a Zn pellet at the bottom and irradiated separately under the same conditions used above. As the laser power was increased, the Au NP solution went from pale pink to deep pink, while the ZnO NPs solution went from pale gray to pale yellow. To prepare Au/ZnO NCs, different volumetric ratios for Au NPs with ZnO NPs (1:3, 1:1, and 3:1 *v/v*) were used. After mixing two colloidal solutions, the second harmonic laser pulses of 800 mJ for 100 pulses were directed at the surface of the solution. The wavelength of the laser used was 532 nm.

2.3. Characterization of NPs

TEM (ZEISS LEO 912, 100 Kv, Oberkochen, Germany) was used to investigate the morphology. ImageJ software (Java 1.8.0, Gaithersburg, MD, USA) was used to determine the diameter of the particles that were synthesized at the nanometer scale. A double-beam UV-vis spectrophotometer (Model 1200, Shimadzu, Kyoto, Japan) was utilized to characterize the prepared nanoparticles in the spectral range of 200–1000 nm. X-ray diffraction analysis (XRD) was performed using the XRD-6000 (Shimadzu, Japan) to confirm the crystal structure of the nanoparticles. The formation of nanoparticles was confirmed using the FTIR spectrum of analyses, conducted using the IFS 48 spectrometer (Bruker, Germany) with a KBr pellet in the range of 4000–500 cm^{-1} .

2.4. Antibacterial Activity of NPs

This experiment was carried out using the agar well diffusion method against *Escherichia coli* (*E. coli*), which was generously provided by the Laboratory of Microbiology at the Division of Biotechnology, Department of Applied Sciences, University of Technology, Baghdad, Iraq. *E. coli* was identified using conventional laboratory protocols [17,18]. The morphology of *E. coli* was studied using scanning electron microscopy (SEM) analysis [19]. The cytotoxic potential against *E. coli* was investigated using an acridine orange/ethidium bromide staining assay [20]. For antibacterial activity, different volumetric ratios for Au NPs with ZnO NPs (1:3, 1:1, and 3:1 *v/v*) were used, while for the cytotoxicity assays and other experiments, only a ratio of 1:1 was tested. The mass concentration of the latter ratio was 100 $\mu\text{g/mL}$ for Au NPs, ZnO NPs, and Au/ZnO NCs, respectively.

2.5. Cell Line Culture

The human breast cancer cell line (AMJ13), human esophageal adenocarcinoma cell line (SK-GT4), and human breast normal cell line (MCF-10) cells were kindly provided by the cell bank unit of the Experimental Therapy Department at Al-Mustansiriyah University,

Baghdad, Iraq. RPMI-1640 culture medium was used for the AMJ13 and SK-GT4 cell lines, supplemented with 10% Fetal Bovine Serum, 2 mM of L-glutamine, 20 mM of HEPES, and 100 mg/mL of streptomycin and 100 IU/mL of penicillin, using tissue culture flasks (T 25 cm²; Falcon, MI, USA) in a CO₂ incubator maintained at 37 °C and 5% CO₂ to allow cells to attach and spread. Each confluent monolayer was washed with PBS (phosphate-buffered saline) and detached with Trypsin-EDTA solution to transfer or passage the cell lines, as described in a previous study [21].

2.6. Methyl Thiazolyl Tetrazolium (MTT) Assay

The cytotoxicity of Au NPs, ZnO NPs, and Au/ZnO NCs was tested using a 96-well plate-based MTT assay [22,23]. The seeding density for the cell line was 1×10^4 cells/well, and a confluent monolayer formed after 24 h. The prepared nanoparticles were applied to the cells and observed for their effects. After 72 h of treatment with the prepared nanoparticles, the medium was discarded, then 28 µL of MTT solution, in a concentration of 2 mg/mL, was added, and the cells were incubated for 2.5 h at 37 °C to determine cell viability. The method used was based on one described in a previous study [24]. A microplate reader was used to measure the absorbance at 492 nm. The test was run three times for accuracy. The percentage of inhibition rate for treated cells was calculated using the following equation [25,26]:

$$\text{Inhibition rate(\%)} = \frac{A_c - A_s}{A_c} \times 100$$

where A_c is the optical density of the control and A_s is the optical density of the samples.

After 24 h of incubation at 37 °C, both cell lines were seeded at a density of 1×10^5 cells/mL into 24-well plates and exposed to Au NPs, ZnO NPs, and Au/ZnO NCs for 24 h. After that, cells were stained with crystal violet and incubated at 37 °C for 10–15 min [27]. Then, the cells were washed out of the stain and photographed using an inverted microscope containing a digital camera at 100× magnification to capture high-resolution images.

2.7. Statistical Analysis

For the statistical study, GraphPad Prism 7.0 software (developed by GraphPad and located in San Diego, CA, USA) was used. The data were presented in an unpaired format. Student's t-test, the standard error of the mean (mean ± SD), and a significance level of $p \leq 0.05$ were used to determine whether the results were statistically significant [28].

3. Results and Discussion

3.1. Characterization of NPs

TEM analysis was utilized to analyze the morphology and ImageJ software was used to calculate the size distributions of the prepared Au NPs, ZnO NPs, and Au/ZnO NCs (Figure 1). As seen in Figure 1A, the TEM image demonstrated that majority of Au NPs have spherical shapes, and the histogram of size distribution exhibited a mean size of ~27 nm. Whereas the ZnO NPs were semispherical nanoparticles with fewer aggregations and had a size of ~35 nm (Figure 1B). Despite using the same methodology and experimental conditions, the particle size of Au NPs was found to be smaller than that of ZnO NPs, and this was due to the difference in the physical and chemical properties of both materials. In addition, the particle size of Au NPs being smaller than the size of ZnO NPs may be attributed to the melting point [29]. It is well-known that nanosized materials have a lower melting point which has a small nanoscale. The melting point of gold is 1064 °C, while the melting point of zinc oxide is 1975 °C. Additionally, the surface tension of the liquid medium can affect the size of NPs, Au NPs have a higher surface energy than ZnO NPs, and they are more likely to be stabilized and form smaller NPs in a medium. In contrast, ZnO NPs may have a lower surface energy, leading to the formation of larger NPs. Au/ZnO NCs revealed a high-population core-shell structure with a mean size of ~51 nm and were

observed to be larger in size than Au NPs and ZnO NPs (Figure 1C). Figure 1C shows an Au NP and its surrounding ZnO. It thus confirms that the black dots seen in the TEM images are Au NPs which are surrounded by ZnO, causing the size of nanocomposites to increase. It also suggests that ZnO surrounding Au NPs is polycrystalline in nature, which will be confirmed by XRD characterization.

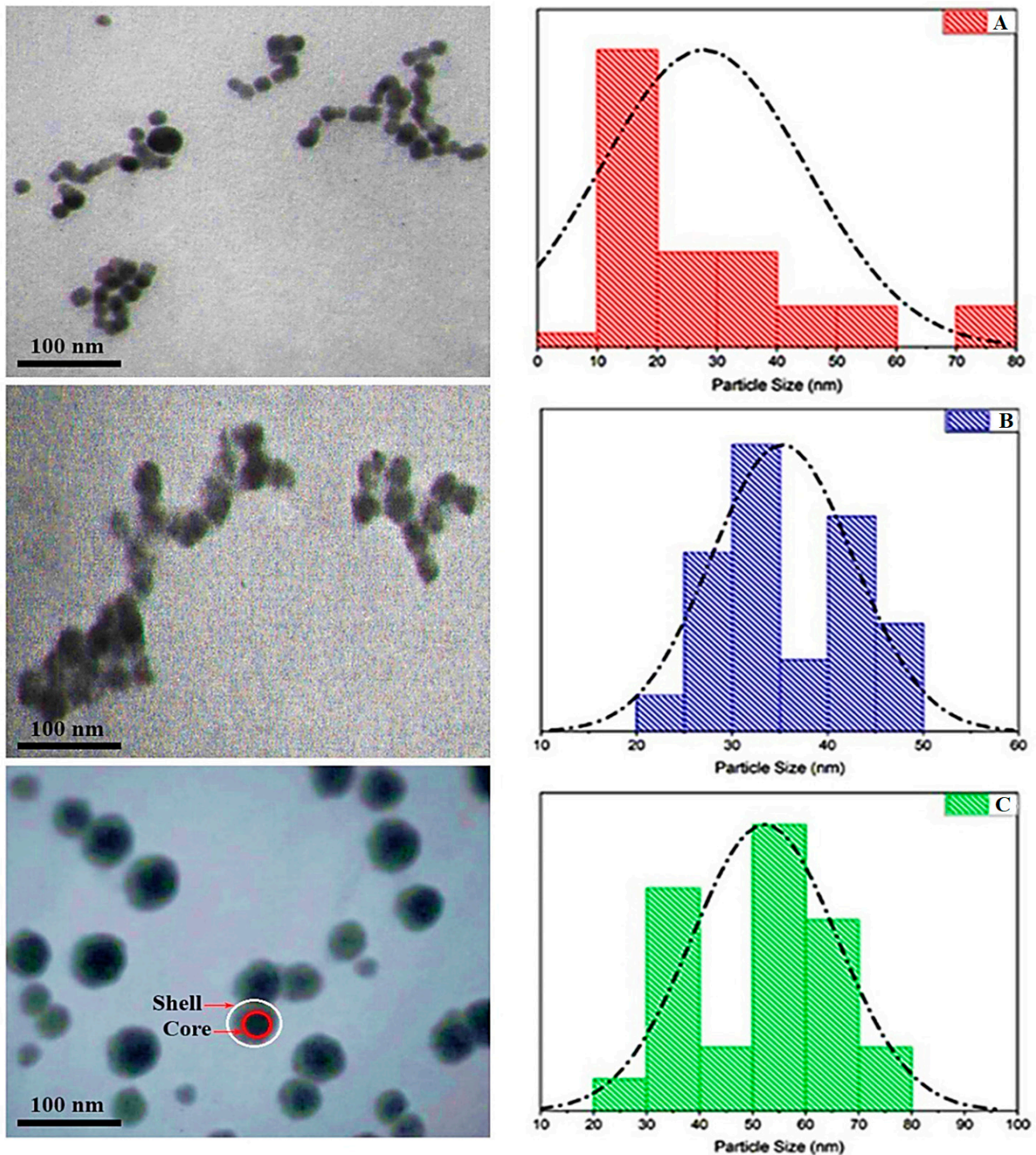


Figure 1. TEM images with particle size distribution histograms of Au NPs, ZnO NPs, and Au/ZnO NCs, where (A) is Au NPs, (B) is ZnO NPs, and (C) is Au/ZnO NCs, prepared via laser ablation at 800 mJ. Core referred to Au and shell referred to ZnO.

XRD is a nanostructure analysis procedure used to determine the crystallinity of metal NPs. XRD is a crucial technique for investigating crystalline structures, since it shows the crystal's atomic arrangement, lattice parameters, and crystalline size [30]. For instance, Figure 2 shows the XRD pattern of Au NPs diffraction peaks at $2\theta = 38.2^\circ$, 44.6° , and 78.2° corresponding to the (111), (200), (220), and (311) planes, respectively, referring to the cubic crystal of the Au NPs. The ZnO NPs were recorded to hexagonal wurtzite and the typical diffraction peaks were at $2\theta = 31.8^\circ$, 34.5° , 36.3° , 48.7° , 57.6° , 63.0° , 68.3° , and 78.7° , corresponding to the (100), (002), (111), (200), (110), (103), (220), and (311) planes. Au/ZnO NCs were shown as a collection of multiple peaks, which was consistent with the JCPDS (Joint Committee on Powder Diffraction Standards) in all respects, with the strongest peak located between 38.2° and 45° , corresponding to the (111) and (200) planes, respectively (00-001-1172). Planes (100), (001), (101), (110), (103), and (112) had diffraction angles of 31.8° , 34.5° , 36.3° , 56.7° , 63.1° , and 68.1° , respectively. These peaks agreed with the JCPDS data and showed that ZnO NP crystals were wurtzite structures (01-079-0205).

UV-vis spectrophotometry was utilized to determine the absorption spectra, concentrations, and types of the prepared NPs. Figure 3 displays the UV-vis absorption of Au NPs, ZnO NPs, and Au/ZnO NCs. The behavior of Au NPs and ZnO NPs was entirely consistent [31]. The strongest peak for Au NPs was at 525 nm, and the color of the colloidal solution was pink due to the surface plasmon resonance. Figure 3 also demonstrates that this peak shifted to red due to aggregation, which produced large ZnO NPs. The blue line represents the absorption peak of ZnO NPs at 410 nm. The Au/ZnO NCs behavior, represented by Figure 3, explained the reduced absorption intensity, compared with absorption intensity for individual elements. Therefore, the intensity absorption peak of Au NPs shifted to 530 nm and that of ZnO NPs shifted to 415 nm. This occurred because the addition of Au NPs to the ZnO NPs matrix significantly reduced the surface plasmon resonance of Au NPs. It is well-known that the size increase of Au NPs causes a red shift of the surface plasmon band. The characteristic plasmon peak of Au/ZnO NCs was observed to be broad in the visible region. This investigation is consistent with the findings of Wang et al. [32].

Au/ZnO NCs samples were examined by FTIR spectroscopy (Figure 4). A peak at 3738 cm^{-1} , corresponding to the symmetrical frequency of water's stretching vibration mode, was used to identify alcohol at (O-H). The presence of carbon dioxide molecules in the air was detected by looking for the C-H bond stretching at a wavenumber of 2353 cm^{-1} . In the nitro compound, the bands at 1516 cm^{-1} corresponded to N-O stretching, whereas the band at 1647 cm^{-1} corresponded to C=C stretching. This was in agreement with a previous study by Liu et al. [33]. Their findings confirmed that the 594 cm^{-1} absorption peak was related to the ZnO metal (ZnO vibrational modes), although it shifted to lower wavenumbers.

3.2. Antibacterial Activity of NPs

The antibacterial activity of Au NPs, ZnO NPs, and Au/ZnO NCs was studied against an *E. coli* strain, dependent on the volumetric ratio for Au NPs with ZnO NPs according to 1:3, 1:1, and 3:1, corresponding to 0.25:0.75, 0.5:0.5, and 0.75:0.25 mL, in addition to the stock samples. As shown in Figure 5, the inhibition zones were measured and reported. In general, the inhibition zone and activity of Au NPs, ZnO NPs, and Au/ZnO NCs against *E. coli* were very active. For more specificity, the mixing ratio (3:1) of Au/ZnO NCs was more efficient than other ratios and more efficient than Au NPs and ZnO NPs alone, which meant that the bacterial membrane grew weaker when a mixture of NPs was applied. Therefore, the inhibition zones were bigger. The mechanism of inhibition by NPs depended on multiple parameters and was strongly affected by the morphology, shape, and size of NPs, in addition to the kind of bacterial strain [34]. NPs can interact with bacterial strains in both physical and chemical methods.

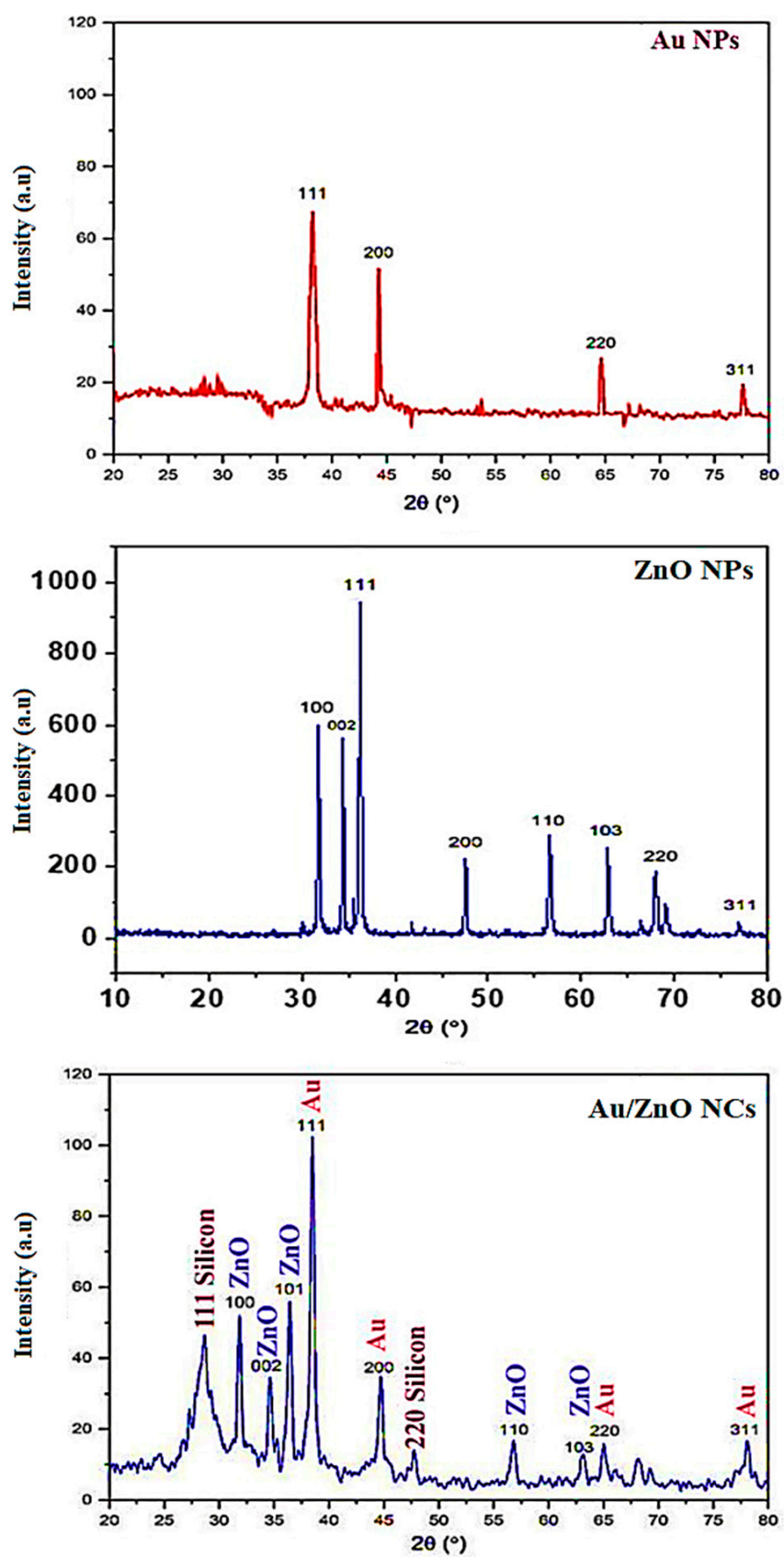


Figure 2. XRD spectra of Au NPs, ZnO NPs, and Au/ZnO NCs prepared via laser ablation at 800 mJ.

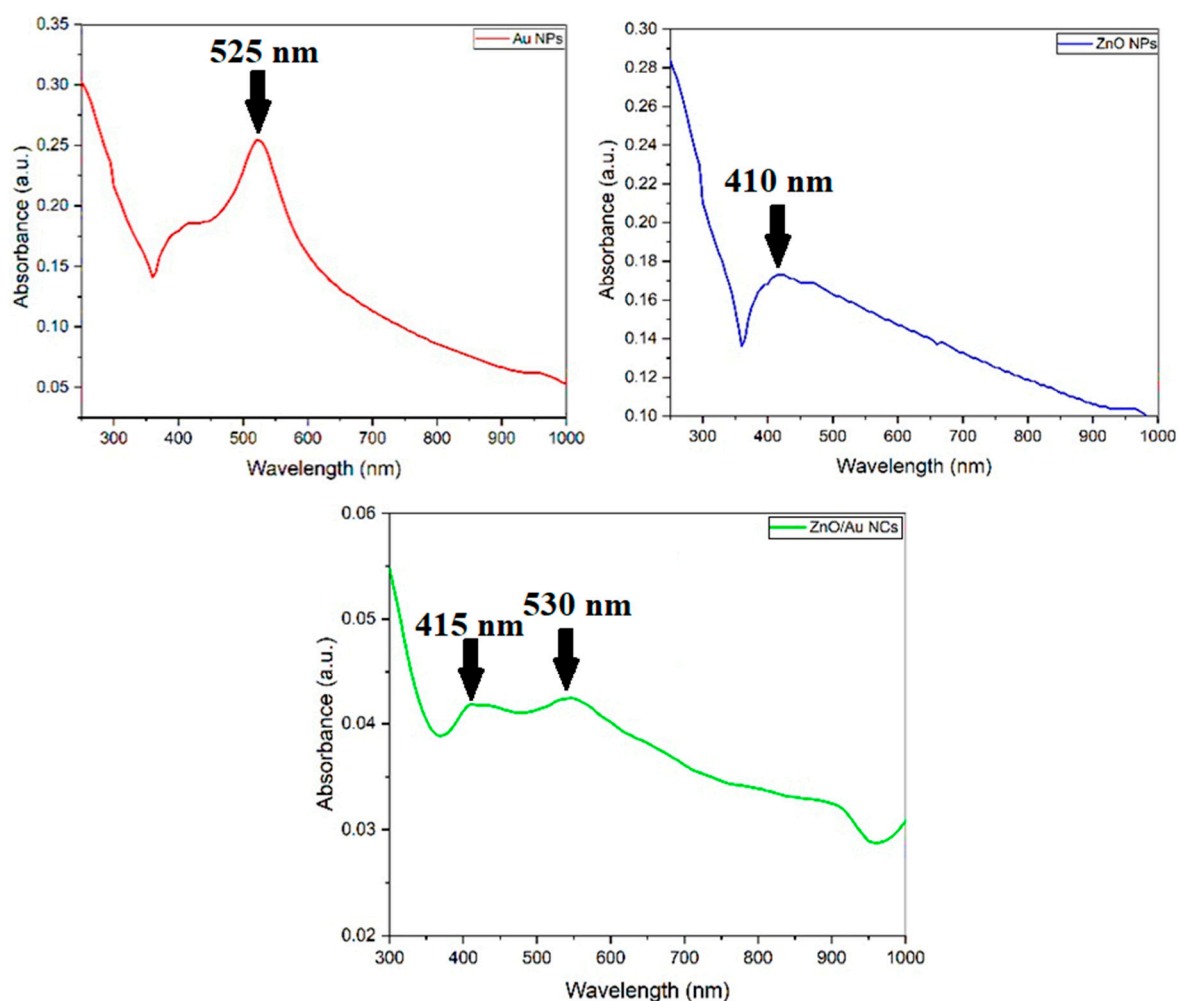


Figure 3. UV-vis spectroscopy of Au NPs, ZnO NPs, and Au/ZnO NCs, prepared by LA at 800 mJ.

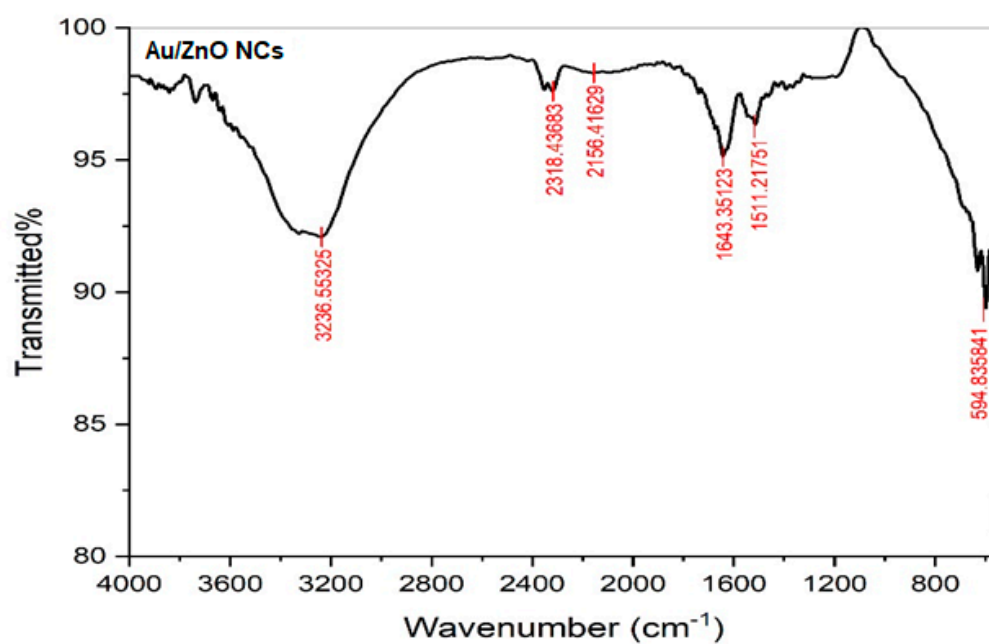


Figure 4. FTIR spectrum of Au/ZnO NCs prepared by LA at 800 mJ.

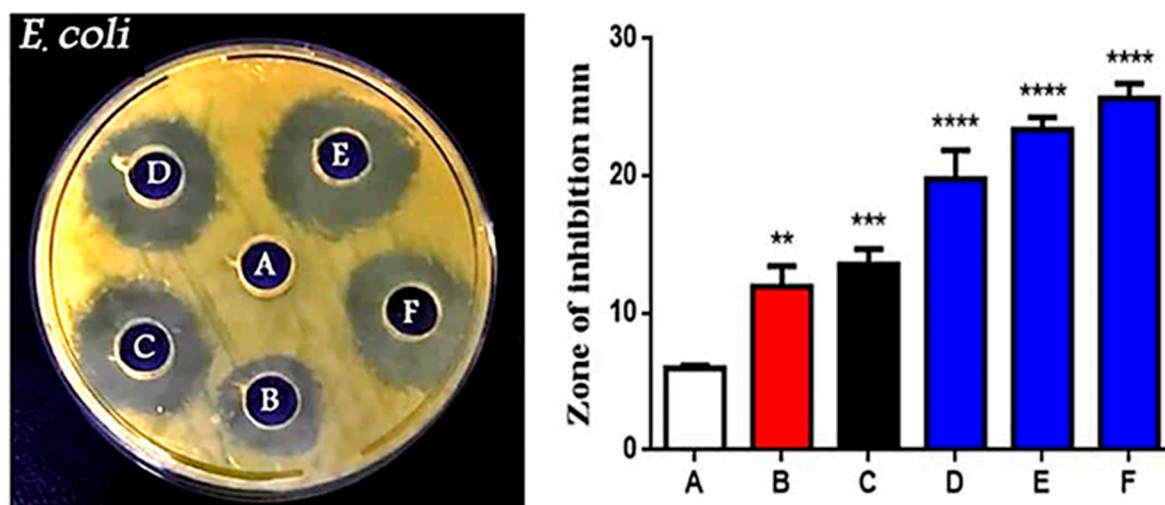


Figure 5. Antibacterial activity of ZnO NPs, Au NPs, and Au/ZnO NCs against *E. coli*. A, non-treated control bacteria; B, treated with ZnO NPs; C, treated with Au NPs; D, treated with Au/ZnO NCs ratio (1:3); E, treated with Au/ZnO ratio (1:1); F, treated with Au/ZnO ratio (3:1). Values are shown as the mean \pm SD of measurements taken in triplicate. ** $p \leq 0.01$, *** $p \leq 0.001$, **** $p \leq 0.0001$.

Due to electrostatic interactions, Zn^{2+} ions are able to enter more easily in *E. coli* bacteria, which have a larger negative charge than *S. aureus* bacteria, resulting in enhanced uptake of ions [35]. Direct physical interactions may take place between bacteria cells and ZnO or Au NPs when the two are in close proximity to one another. These interactions may result in the neutralization of surface electric charge, the deterioration and deformation of the membrane, and changes in the membrane's penetrability. In extreme cases, the membrane may even rupture, resulting in the leakage of cytoplasmic contents and causing the death of the bacteria. ZnO is positively charged, whereas ZnO/Au materials have a slight negative charge [36]. These electrical interactions between the two types of materials are distinct from one another. There is also the possibility that ZnO and Au NPs could exert their antimicrobial effects via reactive oxygen species (ROS), such as superoxide anions or hydrogen peroxide [37–39]. Aquatic ZnO and ZnO/Au dispersions promoted severe oxidative stress and destroyed cellular components such as lipids, proteins, enzymes, and DNA [40]. This was caused by the increased level of ROS that they created. It was demonstrated that Au NPs with tiny dimensions could stimulate the creation of holes in the membrane of *E. coli* via the ROS mechanism, and that after internalization, *S. aureus* could experience an increase in the concentration of intracellular ROS species when exposed to Au NPs [41,42]. The high surface area to volume ratio that was observed for all the produced nanostructures led to the production of a greater number of reactive oxygen species. In addition, ZnO crystals have a diverse chemical composition, which may be a factor in the material's enhanced antibacterial action [43].

3.3. Morphology Changes of Bacteria Investigated by SEM

The morphology of bacteria treated with Au NPs, ZnO NPs, and Au/ZnO NCs was examined using SEM. The variations between the cell structure of bacteria treated with NPs and the untreated control bacteria were visible in images captured using a scanning electron microscope. The morphological alterations for *E. coli* structures, showing moderate activity from the Au NPs and ZnO NPs, can be seen in Figure 6. It was clear that the Au/ZnO NCs had a more significant impact on the organisms' outer membranes, and the damage to cell membranes was observed in the treated *E. coli*. In comparison to untreated bacteria, the treated *E. coli* exposed to Au/ZnO NCs exhibited higher aggregation and membrane disruption. Due to the increase in surface tension brought on by the membrane's neutralized surface membrane potential, the SEM investigation of bacterial cell membranes

revealed aberrant structures, membrane rupture, damage, and blebs. Numerous studies recorded bacterial morphological modifications after exposure to ZnO NPs, and SEM was used in these experiments. The antibacterial action of ZnO NPs included direct contact with cell walls, disrupting bacterial cell integrity [44]. ROS production and the release of antimicrobial ions, particularly Zn ions, may also have been involved [45,46].

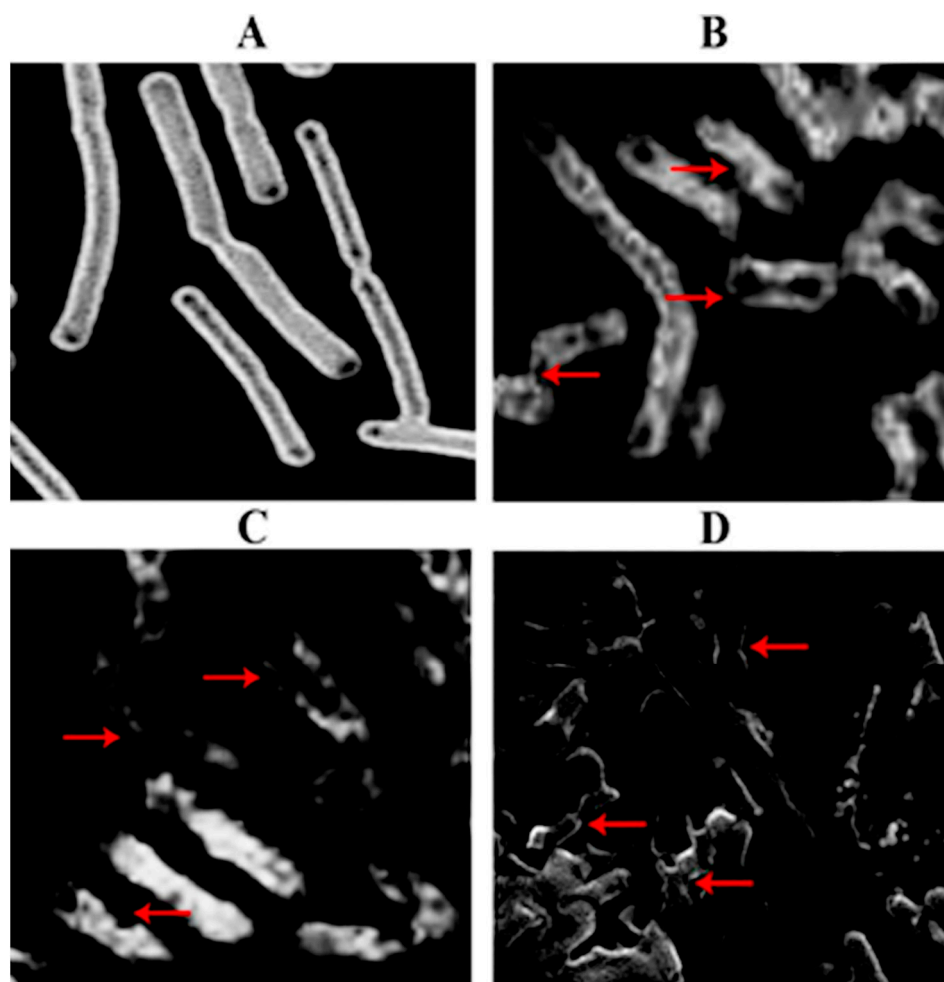


Figure 6. Morphological changes investigated by SEM of *E. coli*. (A) Non-treated *E. coli*, (B) *E. coli* treated with ZnO NPs, (C) *E. coli* treated with Au NPs, and (D) *E. coli* treated with Au/ZnO NCs. Red arrows showing bacterial membrane damage. Scale bar: 1 μm .

3.4. Induces Cell Death of *E. coli*

Fluorescence microscopy was used to assess the antibacterial effectiveness of the produced NPs against *E. coli*. Figure 7 illustrates the use of double staining of acridine orange/ethidium bromide to distinguish between live and dead *E. coli*. When acridine orange attached to the nucleic acid of living bacteria, a fluorescent green light appeared. The red or orange fluorescence of ethidium bromide is caused by its adsorption on the nucleic acid of dead bacteria [47]. Healthy bacterial cells will therefore appear green, whereas dying cells will appear in red. In Figure 7, the results of untreated bacterial cells fluoresced with green color are shown. Following treatment with ZnO NPs, generated at 800 mJ, a number of cells turned red, as depicted in Figure 7B. While in Figure 7C, the bacteria exposed to Au NPs revealed more red color. Both ZnO NP and Au NP treatments alone were sufficient to kill bacteria by damaging their DNA. However, Au/ZnO NCs had a higher effect on bacterial cells than either Au NPs or ZnO NPs alone. In fact, practically all the bacterial cells there turned red, suggesting that more of them died. Hence, Au/ZnO NCs had the greatest impact on both bacterial species. Numerous internal and environmental factors

can lead to DNA damage caused by nanomaterials in bacteria. Internal assaults are one way that ROS can be created. ROS are created during regular cellular metabolism. Due to their great instability, these free radicals react with other molecules quite quickly. Free radicals interact with DNA, triggering a series of events that result in genotoxic lesions. Pharmaceuticals, gamma, ultraviolet, and X-ray radiation are all examples of what are referred to as external agents. Exogenous DNA damage may be caused by NPs.

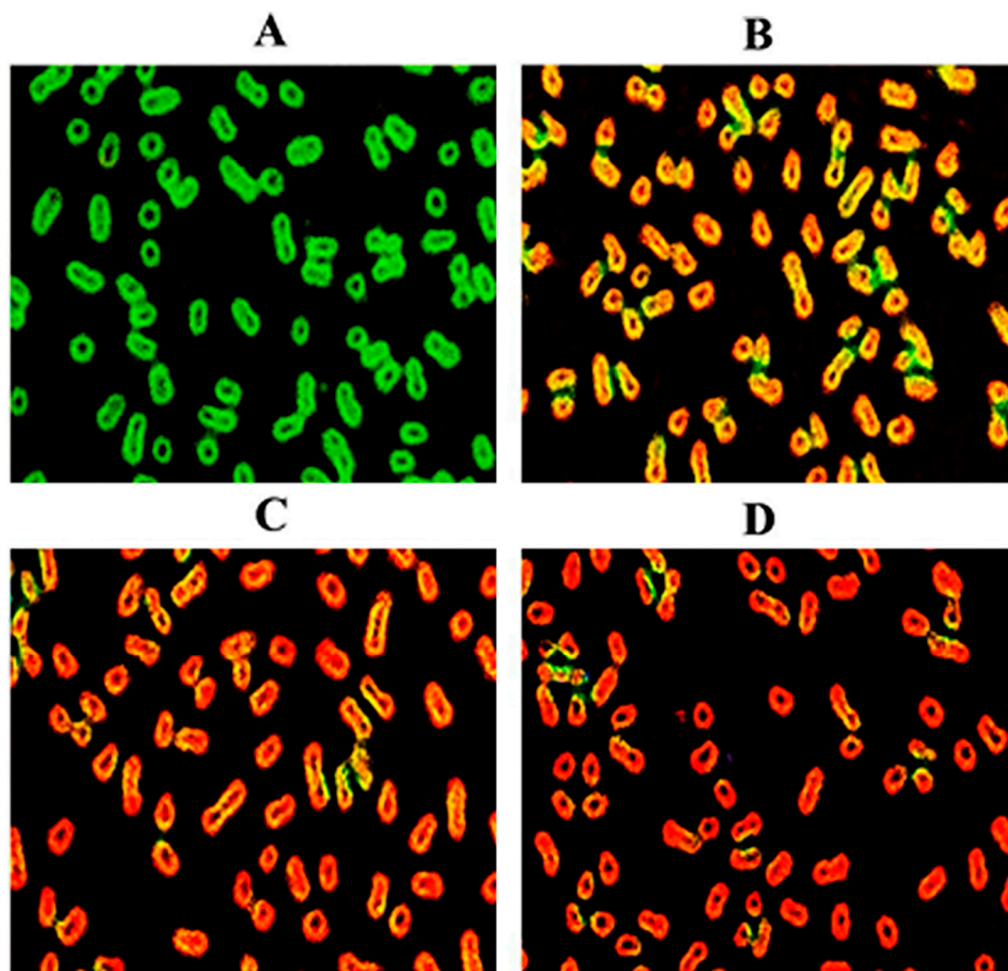


Figure 7. Green and red fluorescence-stained *E. coli* micrographs. (A) Non-treated *E. coli*, (B) *E. coli* treated with ZnO NPs, (C) *E. coli* treated with Au NPs, and (D) *E. coli* treated with Au/ZnO NCs (100×).

3.5. Cytotoxicity of NPs against Cancer Cell Lines

The capacity of Au NPs, ZnO NPs, and Au/ZnO NCs to stop the growth of cancer cells was investigated. The findings demonstrated the cytotoxic effects of Au NPs, ZnO NPs, and Au/ZnO NCs on SK-GT-4, AMJ13, and MCF-10 cells. As shown in Figure 8, AMJ13 cells were used as the test subject for the cytotoxicity of Au NPs, ZnO NPs, and Au/ZnO NCs. The cytotoxicity of Au NPs was higher than 75%, whereas that of ZnO NPs was 70%. The cytotoxicity of Au/ZnO NCs was 89%, which was greater than that of individual Au NPs and ZnO NPs, and excellent for penetrating a cell membrane. The toxicity levels of Au NPs, ZnO NPs, and Au/ZnO NCs toward SK-GT-4 cells were approximately 70%, 68%, and 85%, respectively. However, the Au NPs, ZnO NPs, and Au/ZnO NCs demonstrated less cytotoxic effects against the normal cell line (MCF-10) when compared with those observed in cancer cells. The inhibition rate ranged between 9% and 12%.

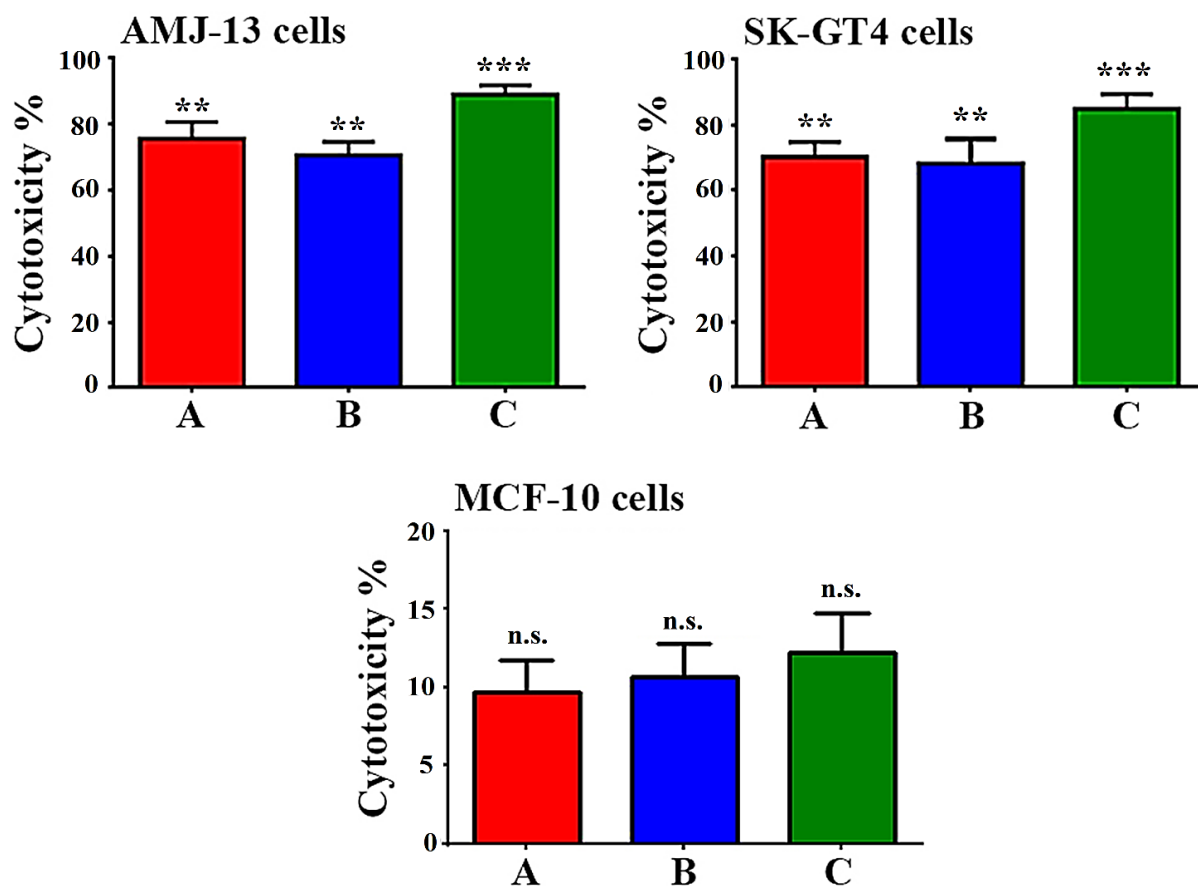


Figure 8. Cytotoxic effects of NPs against AMJ13, SK-GT4, and MCF-10 cell lines. (A) Au NPs, (B) ZnO NPs, and (C) Au/ZnO NCs. Data are represented as mean \pm SD of triplicate. n.s.: non-significant ** $p \leq 0.01$, *** $p \leq 0.001$.

The ability of NPs to act as anticancer agents is diverse, and it strongly depends on the shape, type, and size of NPs, as shown in Figure 9, which represents the morphological changes of the cells when compared with untreated cells (control). Due to their superior activity, spherical Au NPs are preferred over semispherical or randomly shaped ZnO NPs. However, different characterizations and activities can emerge when Au NPs are combined with ZnO NPs to form NPs (Figure 9A–H). In comparison to other nanoparticles, it was discovered that ZnO NPs had a cytotoxic impact that was directed specifically at malignant cells when tested in in vitro conditions. They are capable of undergoing additional surface engineering so that they exhibit greater selective cytotoxicity [48]. ZnO nanoparticles were found to have a cytotoxic effect on many human glioma cells, but no cytotoxic effect was found in normal human astrocytes, as stated in a previous study carried out by Ostrovsky and colleagues [49]. ZnO nanoparticles were found to possess a considerable preferred potential to destroy malignant T cells, according to the findings of another study conducted by Hanley and colleagues [50]. Oxygen is necessary for life, but when it undergoes a redox reaction, it can become a dangerous reactive oxygen species (ROS). ROS are chemically reactive molecules that can either be non-radical or radical. They are created from neutral molecular oxygen (O_2) and are made up of peroxide (O_2^{-2}), oxide (O^{-2}), superoxide (O_2^{-1}), and hydroxyl radical (OH^{-1}). Due to the unique material properties that nanoparticles (NPs) possess, there is a possibility that they could be useful in the fight against cancer. For the purpose of diagnosis and treatment of cancerous tumors, many nanoparticles (NPs), including metal oxide NPs and silver NPs, have been utilized [51]. Zinc oxide nanoparticles, often known as ZnO NPs, have shown significant promise for use in the diagnosis and therapy of cancer cells that have malignant tumors. ZnO

nanoparticles demonstrated excellent biocompatibility and biodegradability, in addition to unique physicochemical properties. ZnO NPs have shown the ability to kill cancer cells by generating reactive oxygen species (ROS) and destroying mitochondria in malignant tumor cells [52]. ZnO nanoparticles are potential candidates to serve as active carriers for the directed and sustained delivery of anticancer medicines into malignant tumor cells [53]. ZnO and TiO₂ are two examples of inorganic heterogeneous catalysts that have a wide variety of applications in the nano-structural, biological, and pharmacological fields [54]. Both these materials, which have wide bandgaps and have a bandgap energy (E_g) of 3.37 and 3.2 eV, respectively, have valence electrons that are able to absorb photons in the high-energy part of the solar spectrum, i.e., UV, and then excite to the conduction band. This is accomplished by using the energy of the bandgap. The findings of the present study suggested that zinc oxide nanoparticles could potentially develop into an anticancer candidate. ZnO nanoparticles exhibit increased cytotoxicity as a result of zinc-mediated protein activity imbalance and oxidative stress [55]. It has been shown that ZnO NPs have the extraordinary capability to generate oxidative stress in cancer cells. This is one of the processes that contribute to the cytotoxicity of ZnO NPs when it comes to cancer cells. ZnO is a semiconducting material, which explains why it has this feature. ZnO causes the production of ROS, which in turn causes oxidative stress, which can ultimately result in cell death if the antioxidative capacity of the cell is overwhelmed [56].

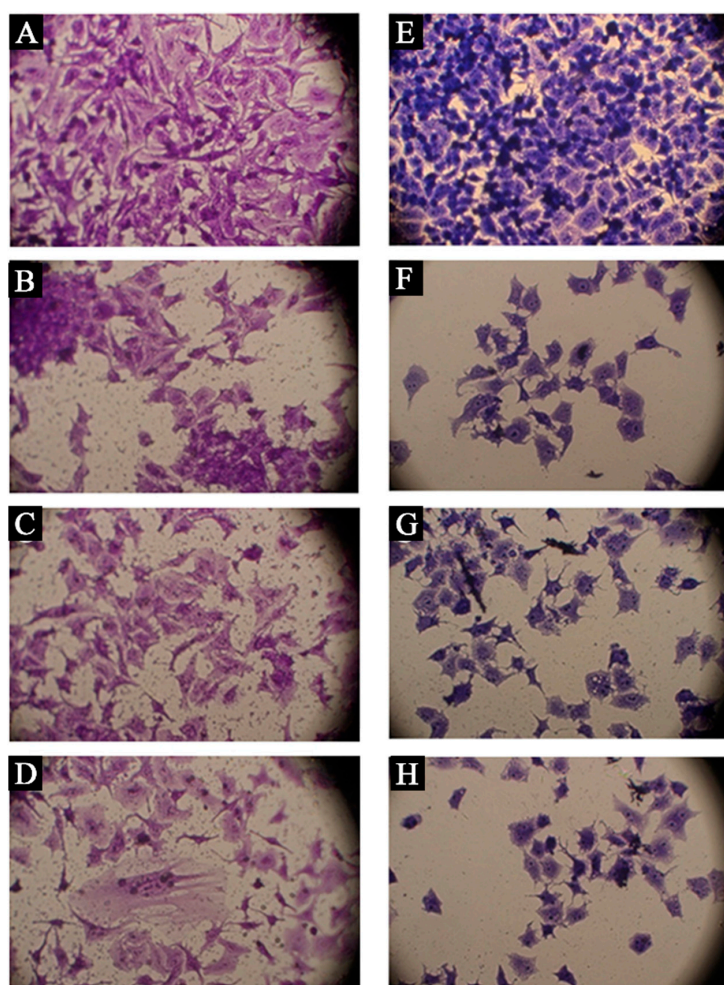


Figure 9. Morphological changes of cancer cells after treatment with the prepared NPs. (A) Non-treated AMJ13 cells, (B) Au NP-treated AMJ13 cells, (C) ZnO NP-treated AMJ13 cells, (D) Au/ZnO NC-treated AMJ13 cells, (E) non-treated SK-GT4 cells, (F) Au NP-treated SK-GT4 cells, (G) ZnO NP-treated SK-GT4 cells, and (H) Au/ZnO NC-treated SK-GT4 cells.

4. Conclusions

Using pulse laser ablation at 800 mJ, a successful preparation of Au NPs, ZnO NPs, and Au/ZnO NCs was produced, which tested for their antibacterial potentials against *E. coli* and their cytotoxic properties against the breast cancer AMG13 cell line and the esophageal cancer SK-GT4 cell line. In the prepared Au/ZnO NCs, the Au NPs were spherical in shape with a size of around 27 nm, and the ZnO was polycrystalline in nature with a wurtzite structure. Compared with the ZnO, the Au/ZnO NCs exhibited increased light absorption and a widened photo-response, indicating that the incorporation of Au NPs with ZnO NPs increased the capacity of UV and visible light absorption, and hence enhanced the photogeneration rate of electrons and holes by light excitation in a wide spectral region. Au and ZnO NPs showed promising antibacterial activity and were more effective when combined as an NC in varying volumes. The results demonstrated that breast cancer cells were shown to be more sensitive than esophageal cancer cells. The proliferation rate of normal breast cells demonstrated a less cytotoxic effect when compared with those observed in cancerous cells. Based on current outcomes, the prepared Au/ZnO NCs could represent a promising strategy for biomedical applications.

Author Contributions: Methodology, M.A., M.S.J., U.M.N., T.M.R., M.I.R., M.A.A.N. and R.J.; software, M.S.J., G.M.S. and K.A.A.K.; validation, G.M.S. and R.J.; formal analysis, G.M.S. and S.F.J.; investigation, M.S.J., T.M.R., G.M.S. and K.A.A.K.; resources, M.S.J., U.M.N., T.M.R. and G.M.S.; data curation, M.S.J., U.M.N., T.M.R. and G.M.S.; writing—original draft preparation, M.A., M.S.J., U.M.N., T.M.R., M.I.R., K.A.A.K. and S.F.J.; writing—review and editing, M.A., M.S.J. and G.M.S.; visualization, M.A., M.S.J. and M.A.A.N.; supervision, M.A., M.S.J., U.M.N. and G.M.S.; project administration, M.A., M.S.J. and G.M.S.; funding acquisition, M.A., M.A.A.N. and K.A.A.K. All authors have read and agreed to the published version of the manuscript.

Funding: The authors extend their appreciation to the Deanship of Scientific Research at the University of Bisha for funding this research through the general research project under grant number: UB-GRP-63-1444.

Institutional Review Board Statement: Not applicable.

Informed Consent Statement: Not applicable.

Data Availability Statement: Not applicable.

Acknowledgments: The authors would like to thank the University of Technology, Phi Nanoscience Center in Baghdad, Iraq, and the University of Bisha, Saudi Arabia, for technical, instrumental, and infrastructural support during this study.

Conflicts of Interest: The authors declare no conflict of interest.

References

- Horikoshi, S.; Serpone, N. *Microwaves in Nanoparticle Synthesis: Fundamentals and Applications*; John Wiley & Sons: Hoboken, NJ, USA, 2013.
- Thomas, S.; Kalarikkal, N.; Oluwafemi, S.O.; Wu, J. (Eds.) *Nanomaterials for Solar Cell Applications*; Elsevier: Amsterdam, The Netherlands, 2019.
- Singh, R.P. Prospects of nanobiomaterials for biosensing. *Int. J. Electrochem.* **2011**, *2011*, 125487. [[CrossRef](#)]
- Jabbar, R.; Sabeeh, S.H.; Hameed, A.M. Structural, dielectric and magnetic properties of Mn²⁺ doped cobalt ferrite nanoparticles. *J. Magn. Magn. Mater.* **2020**, *494*, 165726. [[CrossRef](#)]
- Ayyub, P.; Chandra, R.; Taneja, P.; Sharma, A.K.; Pinto, R. Synthesis of nanocrystalline material by sputtering and laser ablation at low temperatures. *Appl. Phys. A Mater. Sci. Process.* **2001**, *73*, 67–73. [[CrossRef](#)]
- Reich, S.; Schönfeld, P.; Wagener, P.; Letzel, A.; Ibrahimkutti, S.; Gökce, B.; Barcikowski, S.; Menzel, A.; Dos Santos Rolo, T.; Plech, A. Pulsed laser ablation in liquids: Impact of the bubble dynamics on particle formation. *J. Colloid Interface Sci.* **2017**, *489*, 106–113. [[CrossRef](#)]
- Cai, Y.; Zhang, Y.; Ji, S.; Ye, Y.; Wu, S.; Liu, J.; Chen, S.; Liang, C. Laser ablation in liquids for the assembly of Se@Au chain-oligomers with long-term stability for photothermal inhibition of tumor cells. *J. Colloid Interface Sci.* **2020**, *566*, 284–295. [[CrossRef](#)]
- Yang, G.W. Laser ablation in liquids: Applications in the synthesis of nanocrystals. *Prog. Mater. Sci.* **2007**, *52*, 648–698. [[CrossRef](#)]
- Baig, N.; Kamakakam, I.; Falath, W. Nanomaterials: A review of synthesis methods, properties, recent progress, and challenges. *Mater. Adv.* **2021**, *2*, 1821–1871. [[CrossRef](#)]

10. Jiang, T.T.; Qin, X.Y.; Sun, Y.; Yu, M. UV photocatalytic activity of Au@ZnO core-shell nanostructure with enhanced UV emission. *RSC Adv.* **2015**, *5*, 65595–65599. [\[CrossRef\]](#)
11. Rashid, T.M.; Nayef, U.M.; Jabir, M.S.; Falah, A.-H.M. Synthesis and characterization of Au:ZnO (core:shell) nanoparticles via laser ablation. *Optik* **2021**, *244*, 167569. [\[CrossRef\]](#)
12. Jabir, M.S.; Rashid, T.M.; Nayef, U.M.; Albukhaty, S.; AlMalki, F.A.; Albaqami, J.; AlYamani, A.A.; Taqi, Z.J.; Sulaiman, G.M. Inhibition of Staphylococcus aureus α -hemolysin production using nanocurcumin capped Au@ZnO nanocomposite. *Bioinorg. Chem. Appl.* **2022**, *2022*, 2663812. [\[CrossRef\]](#)
13. Shao, X.; Li, B.; Zhang, B.; Shao, L.; Wu, Y. Au:ZnO core-shell nanostructures with plasmon-induced visible-light photocatalytic and photoelectrochemical properties. *Inorg. Chem. Front.* **2016**, *3*, 934–943. [\[CrossRef\]](#)
14. AlMalki, F.A.; Khashan, K.S.; Jabir, M.S.; Hadi, A.A.; Sulaiman, G.M.; Abdulameer, F.A.; Albukhaty, S.; Al-Karagoly, H.; Albaqami, J. Eco-Friendly Synthesis of Carbon Nanoparticles by Laser Ablation in Water and Evaluation of Their Antibacterial Activity. *J. Nanomater.* **2022**, *2022*, 7927447. [\[CrossRef\]](#)
15. Fazio, E.; Go, B.; De Giacomo, A.; Meneghetti, M.; Compagnini, G.; Tommasini, M.; Waag, F.; Lucotti, A.; Zanchi, C.G.; Ossi, P.M.; et al. Nanoparticles engineering by pulsed laser ablation in liquids: Concepts and applications. *Nanomaterials* **2020**, *10*, 2317. [\[CrossRef\]](#)
16. Rashid, T.M.; Nayef, U.M.; Jabir, M.S. Nano-ZnO decorated on gold nanoparticles as a core-shell via pulse laser ablation in liquid. *Optik* **2021**, *248*, 168164. [\[CrossRef\]](#)
17. Bahjat, H.H.; Ismail, R.A.; Sulaiman, G.M.; Jabir, M.S. Magnetic field-assisted laser ablation of titanium dioxide nanoparticles in water for anti-bacterial applications. *J. Inorg. Organomet. Polym. Mater.* **2021**, *31*, 3649–3656. [\[CrossRef\]](#)
18. Mohammed, M.K.; Mohammad, M.R.; Jabir, M.S.; Ahmed, D.S. Functionalization, characterization, and antibacterial activity of single wall and multi wall carbon nanotubes. *IOP Conf. Series. Mater. Sci. Eng.* **2020**, *757*, 012028. [\[CrossRef\]](#)
19. Jihad, M.A.; Noori, F.T.M.; Jabir, M.S.; Albukhaty, S.; AlMalki, F.A.; Alyamani, A.A. Polyethylene glycol functionalized graphene oxide nanoparticles loaded with nigella sativa extract: A smart antibacterial therapeutic drug delivery system. *Molecules* **2021**, *26*, 3067. [\[CrossRef\]](#) [\[PubMed\]](#)
20. Di, T.; Xu, Y.; Liu, D.; Sun, X. Microstructure, Mechanical Performance and Anti-Bacterial Activity of Degradable Zn-Cu-Ag Alloy. *Metals* **2022**, *12*, 1444. [\[CrossRef\]](#)
21. Guidelli, E.J.; Kinoshita, A.; Ramos, A.P.; Baffa, O. Silver nanoparticles delivery system based on natural rubber latex membranes. *J. Nanoparticle Res.* **2013**, *15*, 1–9. [\[CrossRef\]](#)
22. Al-Khedhairi, A.A.; Wahab, R. Silver Nanoparticles: An Instantaneous Solution for Anticancer Activity against Human Liver (HepG2) and Breast (MCF-7) Cancer Cells. *Metals* **2022**, *12*, 148. [\[CrossRef\]](#)
23. Al-Musawi, S.; Albukhaty, S.; Al-Karagoly, H.; Sulaiman, G.M.; Jabir, M.S.; Naderi-Manesh, H. Dextran-coated superparamagnetic nanoparticles modified with folate for targeted drug delivery of camptothecin. *Adv. Nat. Sci. Nanosci. Nanotechnol.* **2020**, *11*, 045009. [\[CrossRef\]](#)
24. Garcia-Mendez, M.C.; Urrutia-Baca, V.H.; Cuao-Moreu, C.A.; Lorenzo-Bonet, E.; Alvarez-Vera, M.; Ortiz-Martinez, D.M.; De la Garza-Ramos, M.A. In Vitro Biocompatibility Evaluation of a New Co-Cr-B Alloy with Potential Biomedical Application. *Metals* **2021**, *11*, 1267. [\[CrossRef\]](#)
25. Kadhim, Z.A.; Sulaiman, G.M.; Al-Shammari, A.M.; Khan, R.A.; Al Rugaie, O.; Mohammed, H.A. Oncolytic Newcastle Disease Virus Co-Delivered with Modified PLGA Nanoparticles Encapsulating Temozolomide against Glioblastoma Cells: Developing an Effective Treatment Strategy. *Molecules* **2022**, *27*, 5757. [\[CrossRef\]](#) [\[PubMed\]](#)
26. Alyamani, A.A.; Albukhaty, S.; Aloufi, S.; AlMalki, F.A.; Al-Karagoly, H.; Sulaiman, G.M. Green Fabrication of Zinc Oxide Nanoparticles Using Phlomis Leaf Extract: Characterization and In Vitro Evaluation of Cytotoxicity and Antibacterial Properties. *Molecules* **2021**, *26*, 6140. [\[CrossRef\]](#)
27. Singh, S.C.; Mishra, S.K.; Srivastava, R.K.; Gopal, R. Optical properties of selenium quantum dots produced with laser irradiation of water suspended Se nanoparticles. *J. Phys. Chem. C* **2010**, *114*, 17374–17384. [\[CrossRef\]](#)
28. Al Rugaie, O.; Jabir, M.S.; Mohammed, M.K.A.; Abbas, R.H.; Ahmed, D.S.; Sulaiman, G.M.; Mohammed, S.A.A.; Khan, R.A.; Al-Regaiey, K.A.; Alsharidah, M.; et al. Modification of SWCNTs with hybrid materials ZnO–Ag and ZnO–Au for enhancing bactericidal activity of phagocytic cells against Escherichia coli through NOX2 pathway. *Sci. Rep.* **2022**, *12*, 17203. [\[CrossRef\]](#)
29. Chavali, M.S.; Nikolova, M.P. Metal oxide nanoparticles and their applications in nanotechnology. *SN Appl. Sci.* **2019**, *1*, 607. [\[CrossRef\]](#)
30. Rashid, T.M.; Nayef, U.M.; Jabir, M.S.; Mutlak, F.A. Study of optical and morphological properties for Au–ZnO nanocomposite prepared by Laser ablation in liquid. *J. Phys. Conf. Ser.* **2021**, *1795*, 012041. [\[CrossRef\]](#)
31. Yang, L.; Yan, W.; Wang, H.; Zhuang, H.; Zhang, J. Shell thickness-dependent antibacterial activity and biocompatibility of gold@silver core-shell nanoparticles. *RSC Adv.* **2017**, *7*, 11355–11361. [\[CrossRef\]](#)
32. Wang, X.; Kong, X.; Yu, Y.; Zhang, H. Synthesis and characterization of water-soluble and bifunctional ZnO–Au nanocomposites. *J. Phys. Chem. C* **2007**, *111*, 3836–3841. [\[CrossRef\]](#)
33. Liu, G.; Swierczewska, M.; Lee, S.; Chen, X. Functional nanoparticles for molecular imaging guided gene delivery. *Nano Today* **2010**, *5*, 524–539. [\[CrossRef\]](#) [\[PubMed\]](#)

34. Mohd Yusof, H.; Mohamad, R.; Zaidan, U.H.; Rahman, A. Microbial synthesis of zinc oxide nanoparticles and their potential application as an antimicrobial agent and a feed supplement in animal industry: A review. *J. Anim. Sci. Biotechnol.* **2019**, *10*, 57. [\[CrossRef\]](#)
35. Huang, Z.; Zheng, X.; Yan, D.; Yin, G.; Liao, X.; Kang, Y.; Yao, Y.; Huang, D.; Hao, B. Toxicological effect of ZnO nanoparticles based on bacteria. *Langmuir* **2008**, *24*, 4140–4144. [\[CrossRef\]](#)
36. Dediu, V.; Busila, M.; Tucureanu, V.; Bucur, F.I.; Iliescu, F.S.; Brincoveanu, O.; Iliescu, C. Synthesis of ZnO/Au Nanocomposite for Antibacterial Applications. *Nanomaterials* **2022**, *12*, 3832. [\[CrossRef\]](#) [\[PubMed\]](#)
37. Jalal, R.; Goharshadi, E.K.; Abareshi, M.; Moosavi, M.; Yousefi, A.; Nancarrow, P. ZnO nanofluids: Green synthesis, characterization, and antibacterial activity. *Mater. Chem. Phys.* **2010**, *121*, 198–201. [\[CrossRef\]](#)
38. Lakshmi Prasanna, V.; Vijayaraghavan, R. Insight into the mechanism of antibacterial activity of ZnO: Surface defects mediated reactive oxygen species even in the dark. *Langmuir* **2015**, *31*, 9155–9162. [\[CrossRef\]](#)
39. Xu, X.; Chen, D.; Yi, Z.; Jiang, M.; Wang, L.; Zhou, Z.; Fan, X.; Wang, Y.; Hui, D. Antimicrobial mechanism based on H₂O₂ generation at oxygen vacancies in ZnO crystals. *Langmuir* **2013**, *29*, 5573–5580. [\[CrossRef\]](#)
40. Sirelkhatim, A.; Mahmud, S.; Seeni, A.; Kaus, N.H.M.; Ann, L.C.; Bakhori, S.K.M.; Hasan, H.; Mohamad, D. Review on zinc oxide nanoparticles: Antibacterial activity and toxicity mechanism. *Nano-Micro Lett.* **2015**, *7*, 219–242. [\[CrossRef\]](#) [\[PubMed\]](#)
41. Badwaik, V.D.; Vangala, L.M.; Pender, D.S.; Willis, C.B.; Aguilar, Z.P.; Gonzalez, M.S.; Paripelly, R.; Dakshinamurthy, R. Size-dependent antimicrobial properties of sugar-encapsulated gold nanoparticles synthesized by a green method. *Nanoscale Res. Lett.* **2012**, *7*, 623. [\[CrossRef\]](#) [\[PubMed\]](#)
42. Zheng, K.; Setyawati, M.I.; Leong, D.T.; Xie, J. Antimicrobial gold nanoclusters. *ACS Nano* **2017**, *11*, 6904–6910. [\[CrossRef\]](#)
43. Kumar, P.; Chiu, Y.-H.; Deng, Z.-I.; Kumar, U.; Chen, K.-L.; Huang, W.-M.; Wu, C.-H. Surface modification of ZnO nanopillars to enhance the sensitivity towards methane: The studies of experimental and first-principle simulation. *Appl. Surf. Sci.* **2021**, *568*, 150817. [\[CrossRef\]](#)
44. Zhang, L.; Jiang, Y.; Ding, Y.; Povey, M.; York, D. Investigation into the antibacterial behaviour of suspensions of ZnO nanoparticles (ZnO nanofluids). *J. Nanoparticle Res.* **2007**, *9*, 479–489. [\[CrossRef\]](#)
45. Li, M.; Zhu, L.; Lin, D. Toxicity of ZnO nanoparticles to *Escherichia coli*: Mechanism and the influence of medium components. *Environ. Sci. Technol.* **2011**, *45*, 1977–1983. [\[CrossRef\]](#) [\[PubMed\]](#)
46. Li, Y.; Zhang, W.; Niu, J.; Chen, Y. Mechanism of photogenerated reactive oxygen species and correlation with the antibacterial properties of engineered metal-oxide nanoparticles. *ACS Nano* **2012**, *6*, 5164–5173. [\[CrossRef\]](#)
47. Palashuddin Sk, M.; Goswami, U.; Ghosh, S.S.; Chattopadhyay, A. Cu²⁺-embedded carbon nanoparticles as anticancer agents. *J. Mater. Chem. B* **2015**, *3*, 5673–5677. [\[CrossRef\]](#)
48. Hanley, C.; Layne, J.; Punnoose, A.; Reddy, K.M.; Coombs, I.; Coombs, A.; Feris, K.; Wingett, D. Preferential killing of cancer cells and activated human T cells using ZnO nanoparticles. *Nanotechnology* **2008**, *19*, 295103. [\[CrossRef\]](#)
49. Ostrovsky, S.; Kazimirsky, G.; Gedanken, A.; Brodie, C. Selective cytotoxic effect of ZnO nanoparticles on glioma cells. *Nano Res.* **2009**, *2*, 882–890. [\[CrossRef\]](#)
50. Hanley, C.; Thurber, A.; Hanna, C.; Punnoose, A.; Zhang, J.; Wingett, D.G. The influences of cell type and ZnO nanoparticle size on immune cell cytotoxicity and cytokine induction. *Nanoscale Res. Lett.* **2009**, *4*, 1409–1420. [\[CrossRef\]](#)
51. Benyettou, F.; Rezgui, R.; Ravaux, F.; Jaber, T.; Blumer, K.; Jouiad, M.; Motte, L.; Olsen, J.C.; Platas-Iglesias, C.; Magzoub, M.; et al. Synthesis of silver nanoparticles for the dual delivery of doxorubicin and alendronate to cancer cells. *J. Mater. Chem. B* **2015**, *3*, 7237–7245. [\[CrossRef\]](#)
52. Anjum, S.; Hashim, M.; Malik, S.A.; Khan, M.; Lorenzo, J.M.; Abbasi, B.H.; Hano, C. Recent advances in zinc oxide nanoparticles (ZnO NPs) for cancer diagnosis, target drug delivery, and treatment. *Cancers* **2021**, *13*, 4570. [\[CrossRef\]](#)
53. Akbarian, M.; Mahjoub, S.; Elahi, S.M.; Zabihi, E.; Tashakkorian, H. Green synthesis, formulation and biological evaluation of a novel ZnO nanocarrier loaded with paclitaxel as drug delivery system on MCF-7 cell line. *Colloids Surf. B Biointerfaces* **2020**, *186*, 110686. [\[CrossRef\]](#)
54. Tanino, R.; Amano, Y.; Tong, X.; Sun, R.; Tsubata, Y.; Harada, M.; Fujita, Y.; Isobe, T. Anticancer activity of ZnO nanoparticles against human small-cell lung cancer in an orthotopic mouse Model ZnO nanoparticles inhibit growth of small-cell lung cancer. *Mol. Cancer Ther.* **2020**, *19*, 502–512. [\[CrossRef\]](#) [\[PubMed\]](#)
55. Shen, C.; James, S.A.; De Jonge, M.D.; Turney, T.W.; Wright, P.F.; Feltis, B.N. Relating cytotoxicity, zinc ions, and reactive oxygen in ZnO nanoparticle-exposed human immune cells. *Toxicol. Sci.* **2013**, *136*, 120–130. [\[CrossRef\]](#) [\[PubMed\]](#)
56. Rasmussen, J.W.; Martinez, E.; Louka, P.; Wingett, D.G. Zinc oxide nanoparticles for selective destruction of tumor cells and potential for drug delivery applications. *Expert Opin. Drug Deliv.* **2010**, *7*, 1063–1077. [\[CrossRef\]](#) [\[PubMed\]](#)

Disclaimer/Publisher's Note: The statements, opinions and data contained in all publications are solely those of the individual author(s) and contributor(s) and not of MDPI and/or the editor(s). MDPI and/or the editor(s) disclaim responsibility for any injury to people or property resulting from any ideas, methods, instructions or products referred to in the content.